TWELFTH EUROPEAN ROTORCRAFT FORUM

Paper No. 25

THE USE OF DISCRETE VORTICES TO PREDICT LIFT OF A CIRCULATION CONTROL ROTOR SECTION WITH A TRAILING EDGE BLOWING SLOT

C.W. HUSTAD

Penguin, a.s Kongsberg Vaapenfabrikk.

Kongsberg, Norway

September 22 - 25, 1986

Garmisch-Partenkirchen
Federal Republic of Germany

Deutsche Gesellschaft für Luft- and Raumfahrt e. V. (DGLR)
Godesberger Allee 70, D-5300 Bonn 2, F.R.G.

THE USE OF DISCRETE VORTICES TO PREDICT LIFT OF A CIRCULATION CONTROL ROTOR SECTION WITH A TRAILING EDGE BLOWING SLOT

C.W.Hustad - Project Engineer,
Penguin Aerostructures Development Group,
a.s Kongsberg Vaapenfabrikk, Norway.

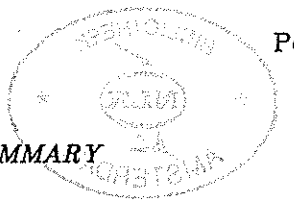

SUMMARY

This paper describes a method which applies discrete vortices to predict the flow around the trailing edge(TE) of a circulation control rotor(CCR) section. The vortices are shed from the blowing lip with a frequency and strength determined by the blowing parameters and lip geometry. As the vortices develop downstream viscosity and entrainment cause vortex growth with eventual overlapping resulting in a pairing process. Once initiated this process breaks down the discrete vortex structure resulting in a large-scale eddy flow representative of the flow in the wake of the CCR section. The proposed model shows distinct similarities with the observed flow field and it is suggested that discrete vortex modelling may offer an alternative, or at the very least suggest improvements, to the finite difference methods which have been used to predict the *TE Coanda flow.*

NOTATION

C_μ	Blowing momentum coefficient
C_N	Normal force coefficient
c	Section chord length
d	Lip thickness
f	Vortex shedding frequency
H	Angular momentum
h	Slot height
K	Vortex strength decay rate
k	Starting length ratio
$\dot{m}$	Massflow rate in kg/s
N	Number of external vortices
q_t	Tangential velocity on a cylinder
P	Number of discrete vortex pairings
q_∞	Free-stream dynamic pressure
R	Radius
R_c	Reynolds number based on chord
r	Vortex core radius
s	Vortex starting length
t	Age of vortex in seconds
U_∞	Free-stream velocity
V_e	Excess jet velocity ($V_\mu - V_p$)
V_f	Frequency velocity ($= 4\pi hf$)
V_i	Induced velocity at the lip
V_p	Velocity at the lip due to the free-stream
V_s	Induced slot surface velocity
V_μ	Jet exit velocity
v	Induced velocity due to a vortex
x	Distance in chordwise direction
y	Distance normal to the chord
Z	Distance along vortex path
z	Distance from a vortex

Greek Symbols

Γ	Circulation in m^2/s
γ	Vortex strength in m^2/s
ν	Artificial viscosity
θ	Angular position from the blowing slot
ρ	Air density

Subscripts

i	Suffix used for the image vortices
j	Suffix used for the external vortices
o	Stagnation or initial condition
p	Relates to potential flow parameters
μ	Relates to the blowing jet

Abbreviations

CC	Circulation control
CCR	Circulation controlled rotor
DVM	Discrete vortex model
TDC	Top Dead Centre
LE	Leading edge
TE	Trailing edge

1. INTRODUCTION

A circulation-controlled rotor (CCR) shown in Fig.1 is distinguished by its blunt trailing edge (TE) around which the separation point is moved in order to develop lift independent of incidence. This is achieved by varying the strength of a wall-jet which emerges from a spanwise slot on the upper surface.

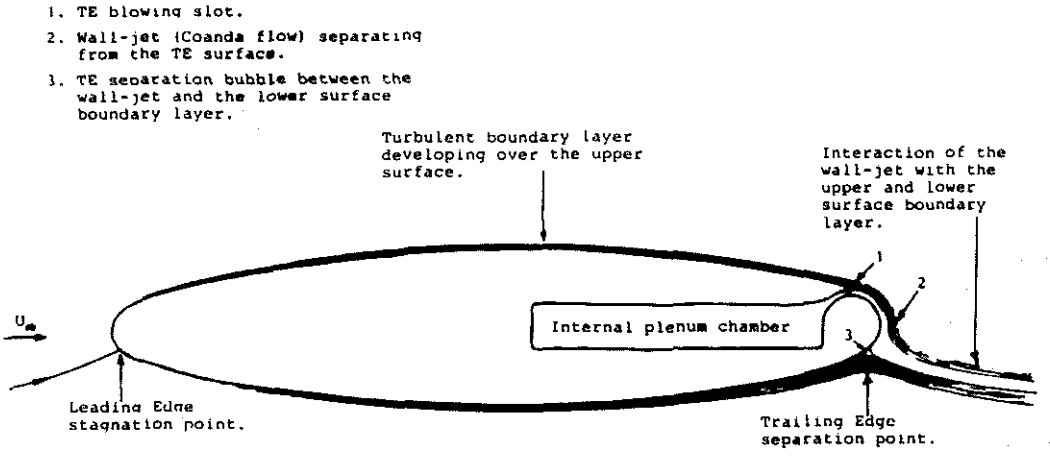

Figure 1. Flow Field around an Elliptic Circulation-Controlled Rotor.

Application of circulation control to future designs extends from simple lift augmentation for fixed wing aircrafts (see for example refs(1) and (2)), through to reducing the mechanical complexity of rotorcraft hubs by using sequential blowing along the blades to compensate for cyclic variation in lift (see refs(3) and (4)).

Prototype projects such as X-wing (see refs(5), (6) and (7)) will be operating with rotors having both trailing and leading edge blowing slots along each blade. This configuration combines the ability of hover in rotary wing mode with high speed cruise capability in the fixed wing-mode.

The lift of a CC-section is dependent upon the TE wall-jet which induces Coanda flow about the TE region. Early experimental work (see for example refs(8) and (9)) showed that performance was dependent on understanding the interaction between the wall-jet and the boundary-layers developing along the upper and lower surfaces. The wall-jet interaction with the upper surface boundary-layer was found to produce a two-phase shear flow, with entrainment and vorticity being dominant features immediately downstream of the lip. Further around, curvature, angular momentum and a radial static pressure gradient determine the streamline pattern and eventual separation from the TE surface due to the oncoming lower surface boundary-layer.

2. THEORETICAL MODELS FOR CIRCULATION-CONTROL

2.1 Early Development Work

One of the earlier theoretical models, suggested by Dunham(10) contained the major elements of the more complex models which have emerged in the last 18 years. It involved calculation of the appropriate potential flow around the body. Superimposed on this was development of the boundary-layer along the lower surface, starting at the LE stagnation point, moving downstream through transition and separation near the rear of the aerofoil. A similar method was applied along the upper surface upto the blowing slot. This resulted in a wall-jet/boundary-layer interaction and required the introduction of correct parameters to get the wall-jet to separate at

the same pressure as the lower surface boundary-layer. If the separation pressures were not the same, new wall-jet parameters were inserted until the iteration loop could be satisfied.

Dunham's model was developed further by Levinsky and Yeh(11) who defined a four-layer wall-jet/boundary-layer velocity profile and introduced expressions for the shear stress distribution together with curvature and induced pressure terms. The results were useful but sensitive to the developing wall-jet profile.

Kind(12) extended Dunham's model to predict the performance of an elliptic CC-section. He revised the initial wall-jet conditions: entrainment, separation and curvature effects. He included an angular momentum equation and developed an empirical expression for the mean static pressure across the jet. However, insufficient experimental data on the turbulent structure within the wall-jet, and dependence on knowledge of the experimental pressure distribution around the trailing edge, restricted the usefulness of the model.

Ambrosiani(13) continued Kind's analysis and developed a self-contained model which did not require such experimental data. He also revised the previously assumed Thwaite's criterion which imposed a constant pressure within the TE separation bubble. Wall-jet separation was formulated using a concept of conservation of mass. The solution involved an iterative matching of an assumed lift coefficient with that calculated from the actual pressure distribution over the section in presence of the TE blowing.

A feature of these early models was the use of integral methods to attempt to model the complex and rapidly changing velocity profiles which existed downstream of the blowing slot. An alternative approach was presented by Gibbs and Ness(14), who applied a finite-difference technique to analyze all the viscous layers around the CC-section. The accuracy of such a model was dependent upon the fineness of the mesh used and its usefulness restricted by computation time which could be excessive when compared with alternative methods of solution.

2.2 Theoretical Model for Incompressible Flow

A combination of the above two techniques was proposed by Dvorak(15) using the computer program CIRCON which was initially developed for incompressible flow. This work was later extended by Dvorak and Kind(16). Their model was applied to arbitrary CC-sections by using a vortex lattice arrangement to generate the potential flow distribution which was used as basis for the boundary-layer development.

Initially the forward stagnation point flow was determined using the Heimenz solution(17). Following this the laminar boundary-layer was calculated using Curle's method(18) with laminar separation being accounted for using correlated data based on measurements by Gaster(19). Transition was predicted using the procedure due to Granville(20), and the initial turbulent value of the shape factor was derived using an empirical relationship based on data obtained by Coles(21).

The integral method of Nash and Hicks(22) was used to calculate the turbulent boundary-layer development along the lower surface up to its separation point. The same method was used for the upper surface development up to the blowing slot, at which point the boundary-layer profile was placed above an almost uniform velocity profile representing the air from the blowing slot. A finite difference technique, which included the effect of surface curvature and transverse pressure gradient, was then used within the wall-jet. The model accounted for viscous effects by including eddy viscosity based on: intermittency, mixing length arguments and Reynolds shear-stress terms.

Results were encouraging but sensitive to the wall-jet parameters and required the use of some semi-empirical expressions.

2.3 Theoretical Model for Transonic Flows

To take account of compressibility Dvorak and Choi(23) extended the above programme with TRACON for application to transonic CC-sections. This applied a flow code due to Jameson(24) for the potential flow calculation which was used as basis for the boundary-layer analysis.

The laminar boundary-layer was calculated using Cohen-Reshotko's method described by Brune and Manche(25). After transition, either through natural transition or due to a separation/reattachment process, Greens method (26) was used for calculating the downstream turbulent boundary-layer development. This was an integral method which used three main differential equations: momentum-integral, entrainment and a rate equation for the entrainment coefficient. These were solved by the Runge-Kutta method until separation or (on the upper surface) the blowing slot was reached.

The calculation method for the wall-jet included the x-momentum, energy and continuity equations which were treated using a finite difference scheme of the Crank-Nicholson type.

Prediction of the pressure distribution concurred with experimental results for both low and transonic speeds at negative angles of attack. However, the model was insensitive to variations of the TE surface and also unable to resolve the flow downstream of a choked blowing slot.

2.4 The Application of Discrete Vortices

An alternative approach was suggested by Smith(27) using discrete vortices to approximate shear between the boundary-layer and wall-jet emerging tangential to the surface of a cylinder in a free-stream.

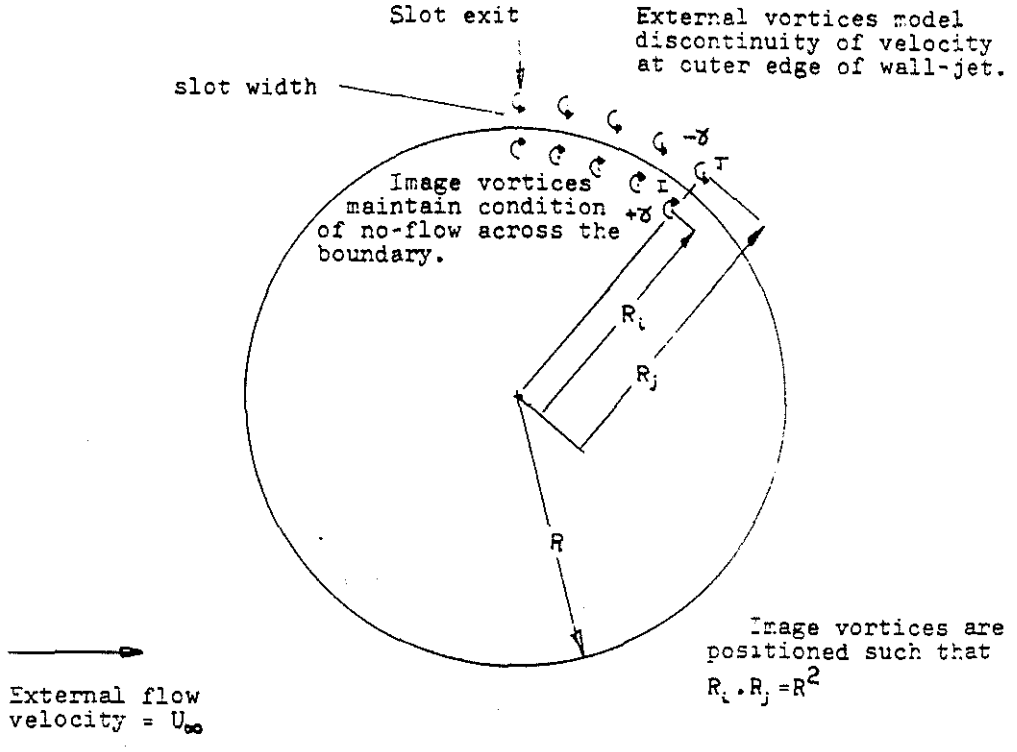

Figure 2. The Discrete Vortex Model Proposed by Smith(27).

Smith included a brief history of discrete vortex modelling with numerous references showing that the technique had been used in treating a variety of two-dimensional shear layer problems. Smith's proposal was a theoretical model for a circular cylinder with a blowing slot at top dead centre (TDC) as shown in Fig.2.

Discrete vortices, with a strength related to the blowing coefficient, were shed sequentially from the lip with a frequency determined by the time-step of the programme. Before each time-step, image vortices of equal but opposite strength to their respective external vortices were located so as to maintain zero flow across the surface boundary. The velocity vector at each external vortex was calculated by summing the induced velocity due to the remaining vortices and free-stream potential flow. The external vortices were then relocated assuming a constant velocity during the time-step, a new vortex shed from the lip, and respective image vortex location and strength calculated before continuing with the next time-step.

The model stabilised with the convection downstream of a vortex sheet as seen in Fig.3.

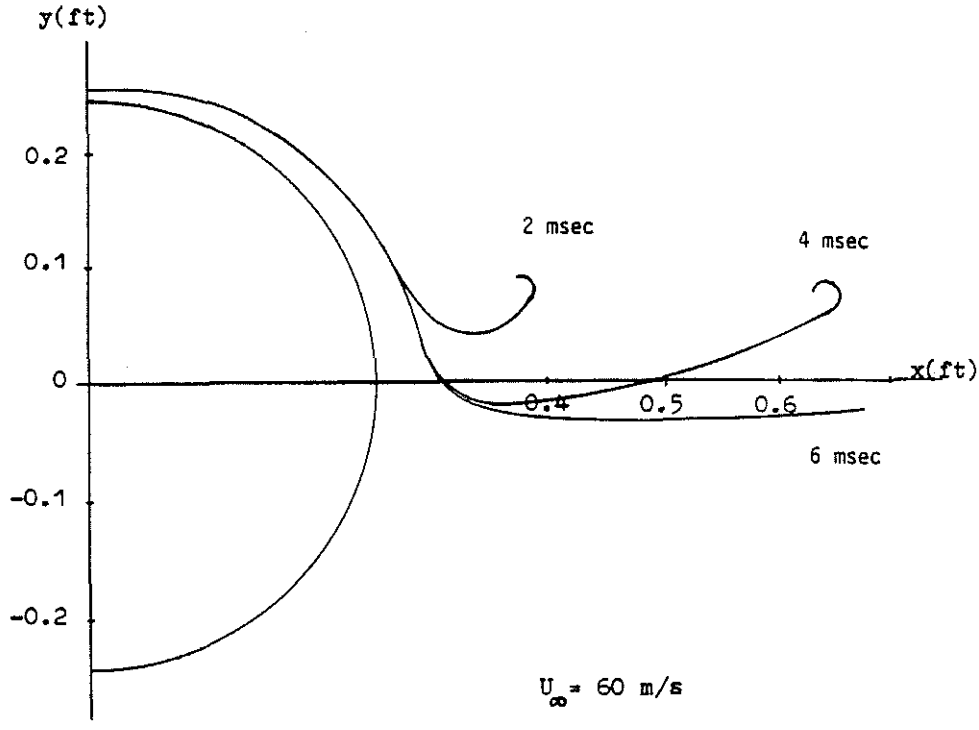

Figure 3. Typical Steady-State Solution of the Model due to Smith(27).

Steady-state solution was dependent upon the initial vortex strength, determined by the velocity difference at the slot. To prevent the model going unstable, Smith introduced artificial viscosity based on the work of Kawahara and Takami(28) who showed that this could be satisfactorily used to stabilise the vortex motion. He also included a vortex strength decay-rate as proposed by Hackett and Evans(29) to take account of entrainment.

Continuation of Smith's work by Soliman(30) et al.(31) clarified some original problems and extended the concept for comparison with elliptic sections. A universal constant value for the decay rate produced similar experimental and theoretical results for several different configurations. However a physical explanation for the inevitable breakdown of the vortex sheet was not included.

Wood and Henderson(32) suggested that the wall-jet/boundary-layer might be considered as a stream of coherent vortices emanating from the lip region as shown in Fig.4.

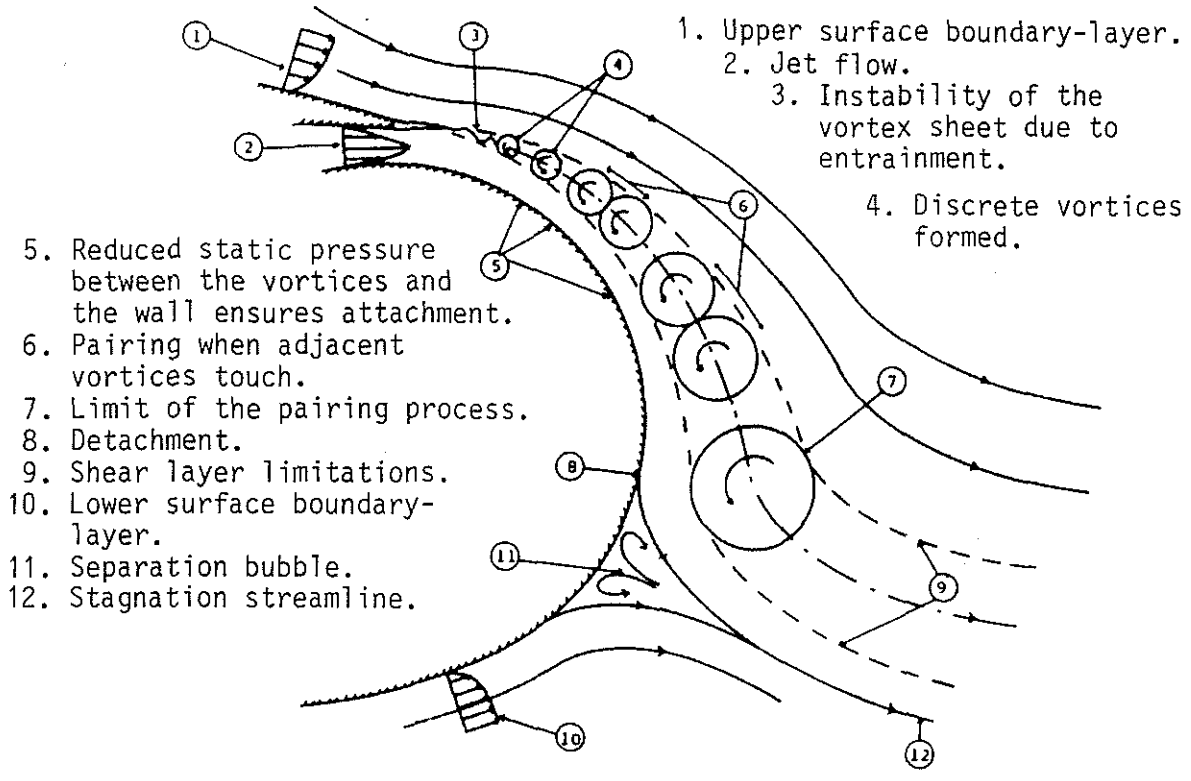

Figure 4. The TE Flow Field as Proposed by Wood and Henderson(32).

Breakdown of the initial shear layer between the wall-jet and upper surface boundary-layer led to the formation of discrete vortices with a frequency dependent on slot geometry and the jet-blowing momentum. Entrainment caused vortex growth with an eventual breakdown of the vortex stream due to pairing when adjacent vortices touched.

3. THE DISCRETE VORTEX MODEL

3.1 Model Development

The model presented in this paper was developed using the original vortex modelling concept suggested by Smith(27) in conjunction with the flow field proposed by Wood and Henderson(32).

The model was originally applied to a cylinder similar to the experimental work of Levinsky and Yeh(11). This was later extended to a 20% elliptic CC-section which was similar to the experimental work of Wood(33).

3.2 The Initial Blowing Parameters

The proposed flow field suggested that the vortex sheet, formed at the lip due to the shear between the jet and upper surface boundary-layer, rapidly broke down and rolled up to form a discrete vortex as shown in Fig.5. This passed downstream leading to a new vortex being formed by the vortex sheet thus resulting in vortex shedding, with a specific frequency, emanating from the lip.

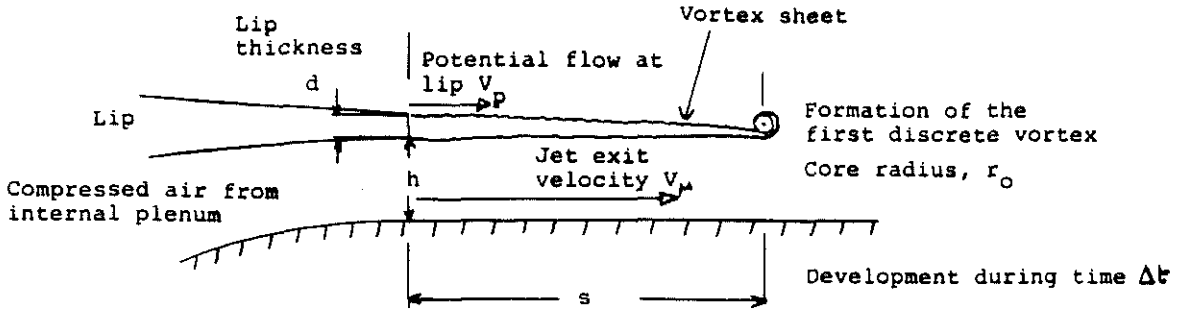

Figure 5. The Breakdown of the Shear Layer at the Blowing Lip.

Considering a slot height h, with a blowing coefficient C_μ resulting in a jet velocity V_μ then

$$C_\mu = \frac{\dot{m}(V_\mu - V_p)}{q_\infty c} \qquad 1$$

where $\dot{m}$ is the mass flow rate in kg/s per unit span and V_p the free-stream potential flow velocity at the lip. Expanding equation(1) and considering incompressible flow where the free-stream and jet exit densities are equal, leads to

$$V_\mu = \frac{V_p + \sqrt{V_p^2 + 2C_\mu/h}}{2} \qquad 2$$

Let s be the length of the vortex sheet before it breaks down to form the first discrete vortex with strength[1] $-\gamma_o m^2/s$. This is relocated at the lip as shown in Fig.6.

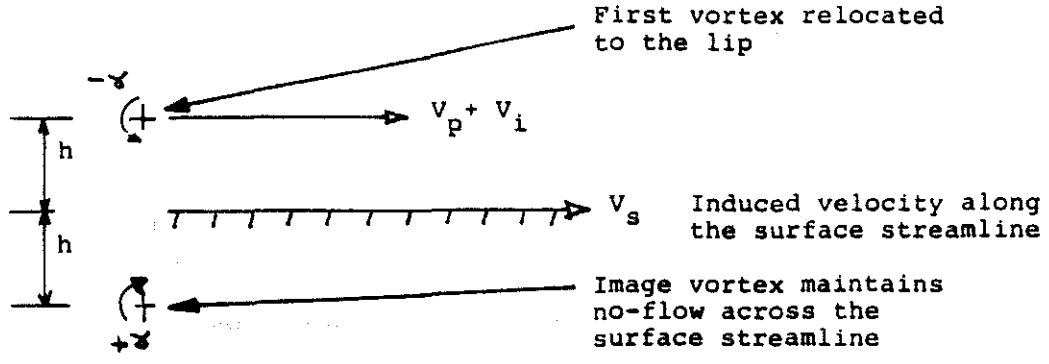

Figure 6. The First Vortex together with its Image Vortex.

To maintain the flow boundary conditions an image vortex must be located inside the surface.

1. Vortex strength is positive when rotation is clockwise.

The induced velocity at the lip due to the image vortex is

$$V_i = \frac{\gamma_0}{4\pi h} \tag{3}$$

where γ_0 is the strength of the image vortex and 2h an approximation to the distance between the lip and the image vortex location.

The starting length s can be related to the time-step Δt by

$$s = (V_p + V_i)\Delta t \tag{4}$$

Defining the excess jet velocity by $V_e = V_\mu - V_p$ and assuming that the vorticity along the sheet is rolled into a concentrated vortex, then

$$\gamma_0 = V_e s \tag{5}$$

Substituting frequency f, with the inverse of time-step $(1/\Delta t)$ and for convenience using an equivalent frequency velocity

$$V_f = 4\pi h f \tag{6}$$

leads to

$$\gamma_0 = V_p \frac{V_e}{(V_f - V_e)} \frac{V_f}{f} \tag{7}$$

hence relating initial vortex strength with frequency.

The relationship between the vortex core radius r_0 and the starting length s is critical in determining the frequency f. The simplest relationship satisfying the boundary conditions is

$$\frac{r_0}{s} = k \tag{8}$$

where k is constant and the core diameter $(2r_0)$ is similar in magnitude to the lip thickness.

The resulting relationship for frequency has two terms

$$f = \frac{kV_p}{r_0} + \frac{V_e}{4\pi h} \tag{9}$$

where the first term is considered to be a threshold frequency dependent upon free-stream velocity and slot geometry. The second term is a function of blowing strength and slot height.

Increasing slot height h, and lip thickness d, (hence r_0), decreases the shedding frequency. With increasing slot height the frequency augmentation rate df/dC_μ is reduced.

At low slot heights the frequency becomes unrealistically high for the proposed flow regime and it is suggested that the stability of the vortex sheet increases due to the proximity of the surface, thus delaying the roll up into discrete vortices and altering the condition set by equation(8).

3.3 The Starting Process

Having found the initial blowing parameters, the first external vortex is placed at the blowing lip.

The location of the first internal image vortex is such that there is no flow across the surface boundary. This is satisfied around a cylinder when

$$R^2 = R_i R_j \qquad 10$$

The strength of the image vortex is equal but of opposite sign to the external vortex.

The induced tangential velocity at a point P, distance z from a vortex J with strength γ, is

$$v_j = \frac{\gamma}{2\pi z} \qquad 11$$

Substitution in the model of equation(11) rapidly leads to the breakdown of the vortex motion. By applying artificial viscosity as used by Smith to stabilise the vortex development, then the induced velocity is modified to

$$v_j = \frac{\gamma}{2\pi z}\left[1-\exp\left(-\frac{z^2}{4\nu t_j}\right)\right] \qquad 12$$

Where t_j is the age of the j^{th} vortex and ν is the artificial viscosity. Typically $\nu = 0.001$ has provided reasonable damping to the vortex motion. Smith suggested the relationship

$$\nu = \nu_0\sqrt{\gamma_0} \qquad 13$$

where $\nu_0 = 0.013$. This relationship has also been used for the present model.

The iterative process develops by calculating the resultant velocity of the external vortices. This is the sum of the induced velocity due to the remaining external vortices, the internal image vortices and the free-stream potential flow velocity.

After each time-step Δt the vortices are *marched* downstream and a new lip vortex is inserted. The new image vortex locations are then calculated for each respective external vortex.

Typical development of the vortices after 20 iterations is shown in Fig.7 for the case of a cylinder with a TDC blowing slot.

The vortex path curls to form a characteristic spiral starting vortex which is carried downstream before a steady-state solution is reached.

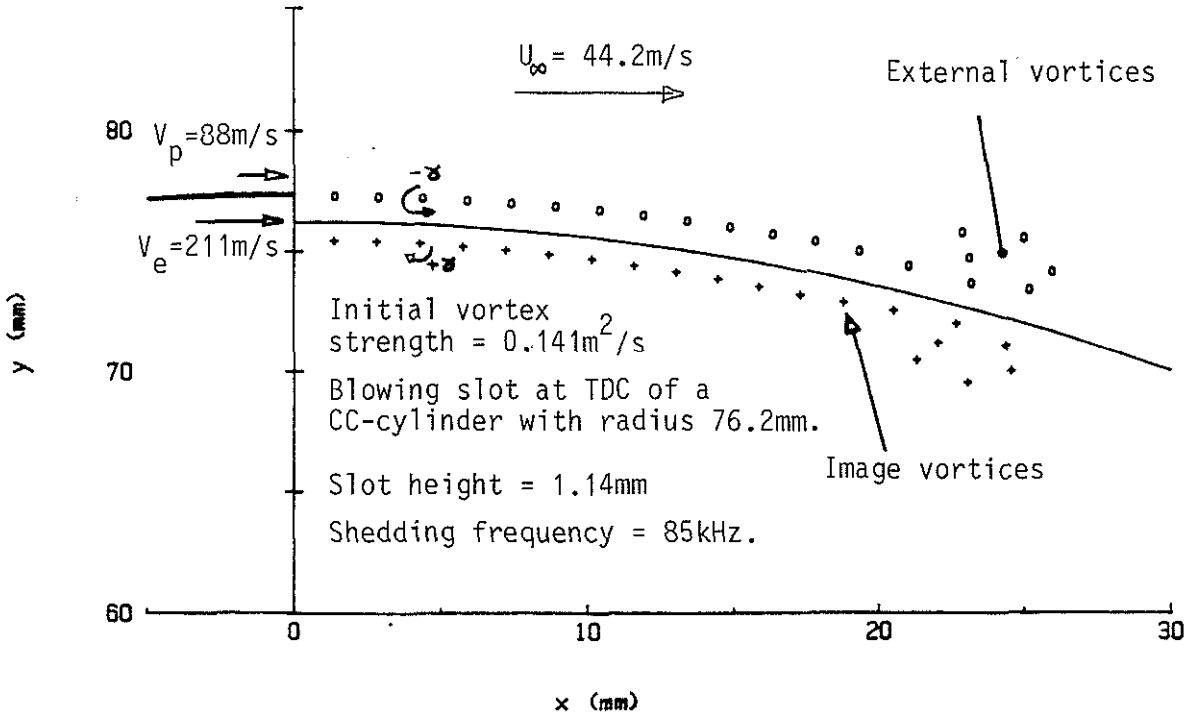

Figure 7. Early Development of the Vortices Downstream of the Blowing Slot.

3.4 Vortex Growth and Pairing

To model flow entrainment the vortex strength is subject to an exponential decay of the form

$$\gamma = \gamma_0 \exp(-Kt) \qquad 14$$

where K is a decay rate constant[2] and t, the age of the vortex in seconds.

The core size is related to the vortex strength by assuming a conservation of angular momentum H, so that

$$H = \gamma_0 r_0^{\,2} = \gamma r^2 \qquad 15$$

From equation(14)

$$r = r_0 \exp(Kt/2) \qquad 16$$

This results in a gradual increase of the vortex size as they pass downstream.

Eventual overlapping of the vortices starts a pairing process which assumes a summation of the cross-sectional core area and conservation of angular momentum.

2. Typical value used is K=100.

For pairing between the j^{th} and $j+1^{th}$ vortex the new radius is given by

$$r' = \sqrt{r_j^{\,2} + r_{j+1}^{\,2}} \qquad 17$$

and new strength by

$$\gamma' = \frac{\gamma_j r_j^{\,2} + \gamma_{j+1} r_{j+1}^{\,2}}{r'^{\,2}} \qquad 18$$

The new position is such that the distance to the new vortex location x is inversely proportional to the original radii for both vortices, if x is the distance from a colinear datum then

$$x' = \frac{x_j r_j + x_{j+1} r_{j+1}}{r'} \qquad 19$$

3.5 Lift Prediction

It is shown in appendix-A of ref(34) that the tangential velocity at a point P on the circumference of a cylinder under the influence of an external discrete vortex and its image vortex is given as

$$q_t = \frac{\gamma}{2\pi R}\left(\frac{A}{B}\right)\left[\frac{1}{1-A\cos\alpha}\right] \qquad 20$$

where

$$A = \frac{2R}{R_j + R_i} \qquad 21$$

and

$$B = \frac{2R}{R_j - R_i} \qquad 22$$

and α is the arc angle subtended from P to the radial line joining the vortex pair.

Using equation(20) it is further shown that the circulation about a cylinder due to a discrete vortex pair (external vortex together with its respective image) is equivalent to the image vortex strength γ. The total circulation due to blowing can therefore be related to the sum of the image vortices within the flow-fields so that

$$\Gamma = \sum_{i=1}^{N} \gamma_i \qquad 23$$

Remembering the relationship Lift $= \rho U_\infty \Gamma$ then the normal force coefficient due to blowing can be expressed independently of incidence effects as,

$$\Delta C_{N(\text{blowing})} = \frac{2}{U_\infty c} \sum_{i=1}^{N} \gamma_i \qquad 24$$

4. *RESULTS AND DISCUSSION*

4.1 Application of the Discrete Vortex Model to a CC-Cylinder

The model was initially developed for a CC-cylinder similar to the experimental work of Levinsky and Yeh(11).[3]

Early work showed that onset of pairing was dependent upon the starting ratio k.[4] Too large a value ($k>0.4$) resulted in pairing starting unrealistically close to the lip, too small a value meant that pairing was not initiated during the computation time. Sensible values for k seemed to lie in the region $0.15 \leq k \leq 0.35$. This implied that the vortices being shed from the lip could have a spacing between 3 to 7 times their core radius.

With the onset of pairing the vortex structure rapidly broke down resulting in weaker, larger vortices disappearing downstream. These were gradually removed from the iterative procedure by means of a downstream *cut-off* line. If any external vortex had passed beyond this line then the end vortex was removed. This led to a gradual unravelling of the characteristic starting vortex.

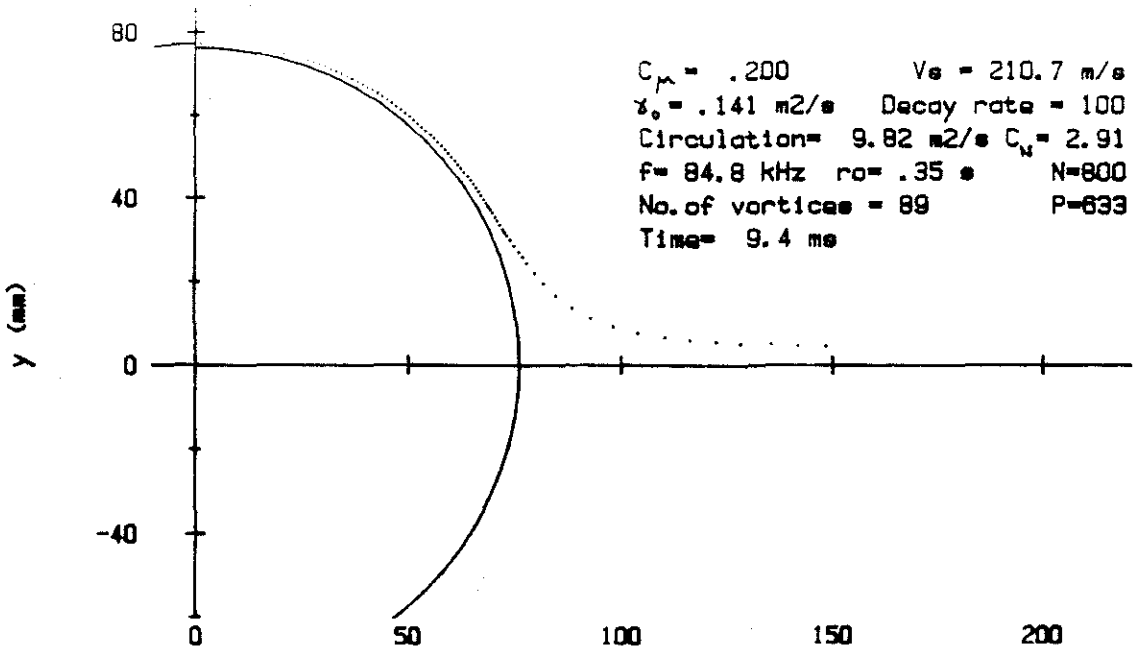

Figure 8. Steady-State Solution of the Proposed DVM for a CC-Cylinder.

A typical steady-state distribution after 9.5ms (800 iterations) is shown in Fig.8. Of the 800 vortices which have been shed from the lip there are 89 left. There have been 633 pairings and 78 vortices have passed downstream of the cut-off line which was set to x = 150mm. The summed strength of the image vortices within the flow field is $9.8 m^2/s$ which applying the relationship in equation(24) leads to a predicted normal force coefficient of 2.9.

---

3. A cylinder of radius 76.2mm with a slot height of 1.14mm submerged in a free-stream velocity of 44.2m/s. There is no information about the blowing lip geometry. A value of 0.8mm was assumed for the lip thickness d, hence r_0=0.4mm has been used.
4. See equation(8).

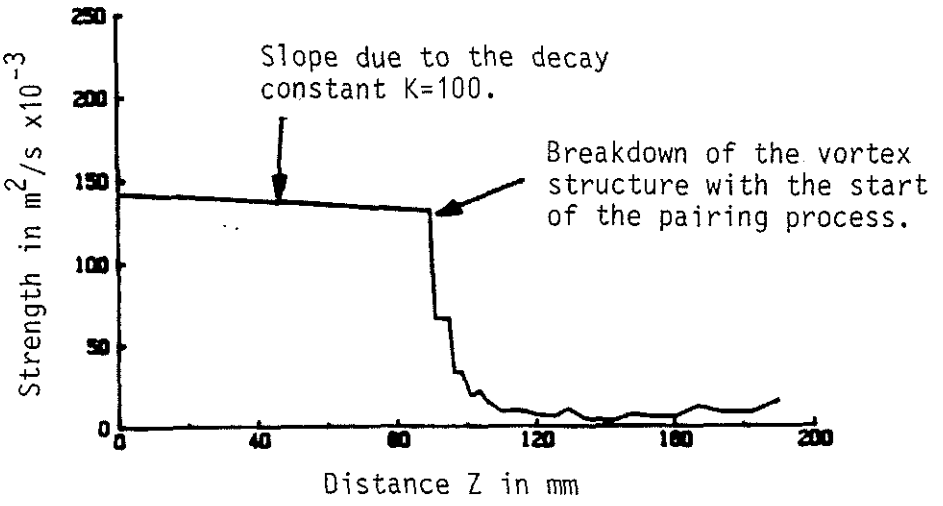

Figure 9. Variation of Vortex Strength in the Wake of a CC-Cylinder.

The breakdown of the vortex structure is shown in Fig.9 where the vortex strength is plotted against distance Z from the lip along the vortex path. Pairing starts about 90mm downstream of the lip and rapidly reduces the vortex strengths.

Fig.10 shows comparison between the present model and the work by Levinsky and Yeh(11) as well as some experimental data by Cheeseman(3) for a similar configuration.

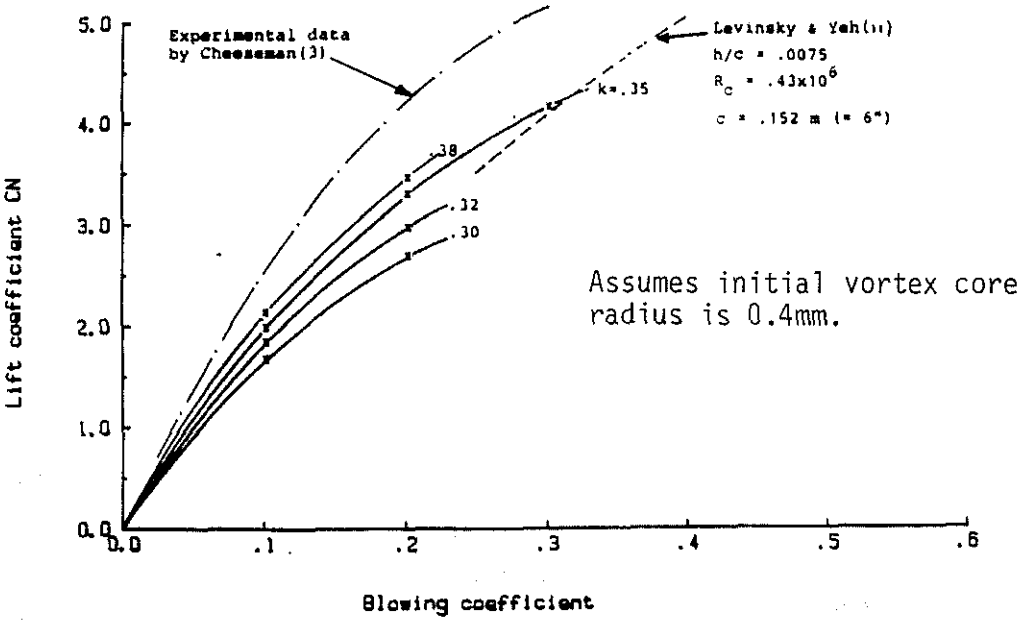

Figure 10. Comparison of the Discrete Vortex Model with Previous Experimental Work.

Reducing the starting ratio k leads to a reduction of the resulting normal force coefficient. A value of k = 0.35 gives reasonable agreement with the experimental results. Assuming a vortex core radius of 0.4mm this suggests the initial vortex sheet at the lip is about 1.2mm in length.[5]

5. These values are very much dependent upon the lip geometry and are only intended to give a rough indication of magnitudes.

4.2 Application of the Discrete Vortex Model to a CC-Ellipse.

Extension of the model to consider the effect of vortex shedding from an elliptic aerofoil was investigated by first considering the potential flow around a cylinder and using conformal transformation to calculate the equivalent flow around an ellipse. The vortices were then shed into the potential flow from the lip.

Positioning of the image vortices had to be slightly modified due to the changing curvature; the criterion being that the line joining the external vortex with its image was perpendicular to the surface at the point of intersection. The radial distance was then calculated by extending this line to the x-axis and using the relationship $R^2 = R_i R_j$ where R was the distance from the x-axis intersection to the surface and R_i, R_j were the respective distances to the image and external vortex.

The 20% elliptic model was developed with a slot at 96.5% chord and a slot height to chord ratio of 0.0012. This was similar to the configuration of Wood(33) and subsequently Hustad(34) on a model with chord of 0.610m with a free-stream velocity of 30m/s.

Preliminary work using a starting ratio of 0.35 and a core radius of 0.2mm (representative of the lip thickness) led to premature pairing. Reducing the starting ratio to 0.25 resulted in a shedding frequency of 45kHz[6] at a blowing coefficient $C_\mu = 0.01$.

An example of the vortex development is shown in Fig.11 after 300 and 500 iterations.

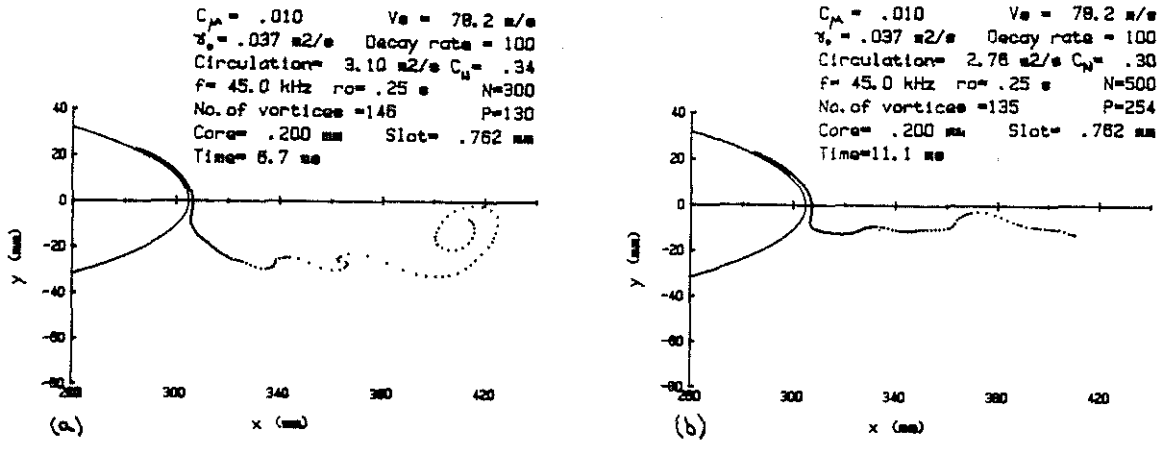

Figure 11. Vortex Development Downstream of an Elliptic CC-section.

Fig.11(a) exhibits two classic features of discrete vortex models; the rolling up of the tail end into a starting vortex, and the tendency of the path to curl into a S-shape. This is a characteristic mode of instability leading to possible breakdown of the vortex path. With the cut-off line set at x = 410mm the programme has begun to unravel the starting vortex by removing the tail vortex following each iteration step.

6. Wood and Henderson(32) suggested a possible shedding frequency of 40-60kHz which was just above their anemometry frequency range.

After 500 iterations, see Fig.11(b), the starting vortex has passed downstream and the TE flow is beginning to approach a *quasi* steady-state solution.

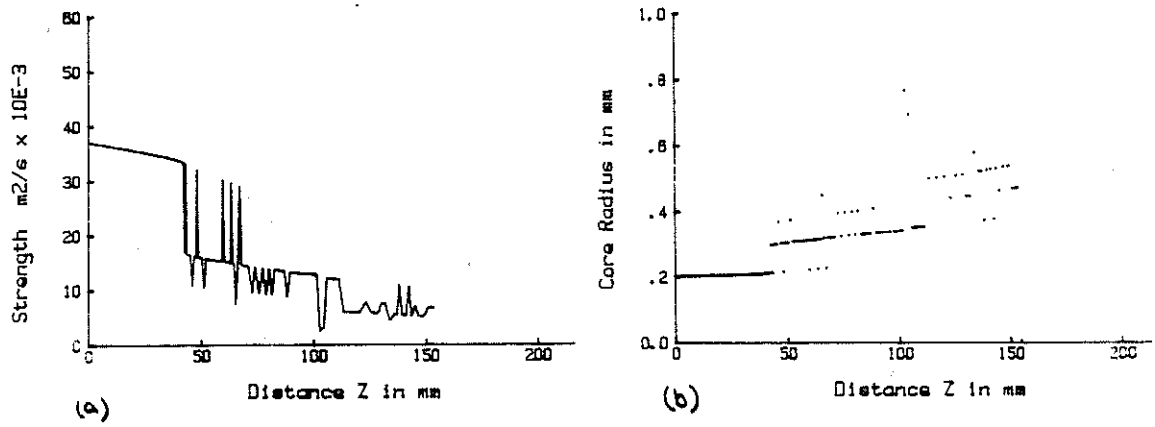

Figure 12. The Breakdown of the Vortices due to the Pairing Process.

Fig.12(a) shows the resultant vortex strength plotted against distance Z along the vortex path. Pairing starts 40mm downstream of the lip. Some of the vortices pass for a short time unpaired before touching their neighbour. The growth of the vortices is shown in Fig.12(b). The core radius has grown 3 to 4 times its original value of 0.2mm and the vortices are by now more representative of a large-scale eddy flow disappearing downstream.

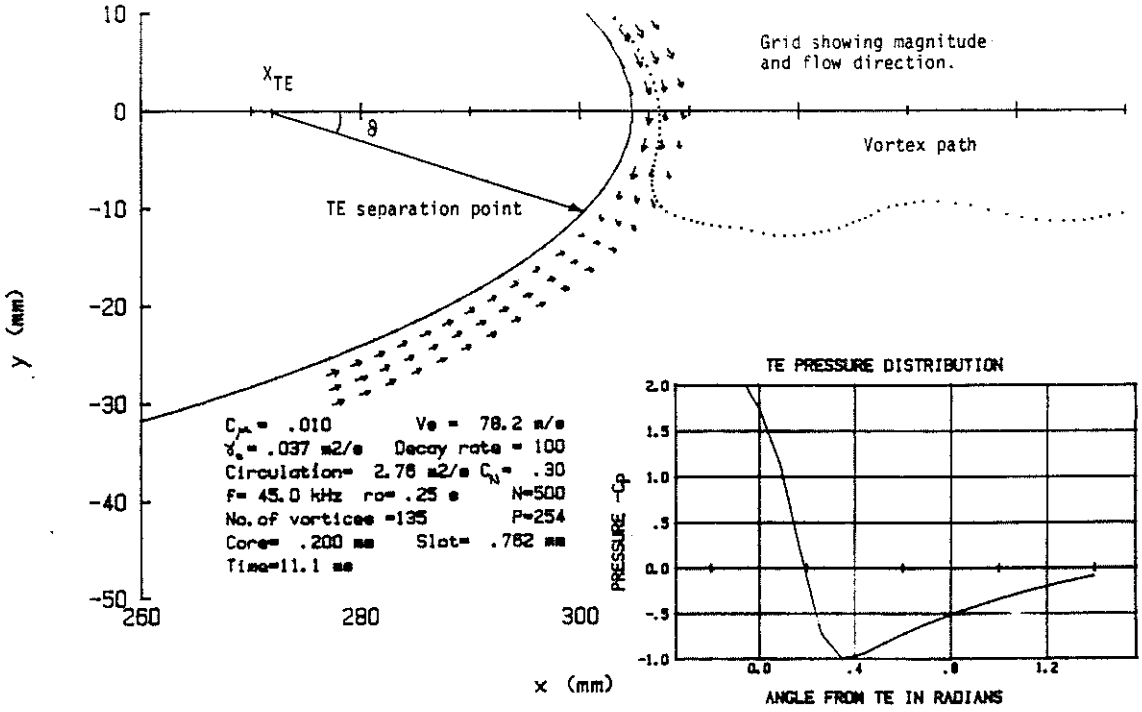

Figure 13. Local Flow Pattern and Pressure Distribution around the TE.

For flow visualization purposes the model was *seeded* with a passive point grid system before the final iteration. These are vortices with zero strength whose velocity and direction reveal the streamline pattern. The grid is distributed about the TE region as shown in Fig.13.[7] The grid lines show the lower surface flow separating together with the upper surface flow which is coming from the blowing slot passed the TE and onto the lower surface.

The TE pressure distribution (shown inset in Fig.(13)) suggests that separation occurs at $\theta = 0.35$rads which based upon conventional potential flow theory would infer a normal force coefficient $C_N = 1.3$. This is not realistic for the configuration shown.[8] However the normal force predicted by summing the internal vortices suggest a value of $C_N = 0.3$ which is in good agreement with the experimental values from refs(33) and (34).

4.3 Limitations and Possibilities of the Proposed Discrete Vortex Model.

The model described in this paper considers only the TE region of the CC-section and is limited to incompressible flow. No account is taken of the boundary-layer development upstream of the TE region nor within the wall-jet.

Preliminary performance results[9] have shown that vortex development is dependent upon an accurate estimate of the initial blowing parameters. There is at the present time very little data relating to the size, strength, shedding frequency and pairing characteristics of the proposed discrete vortices: more experimental work is required for understanding their behaviour.

However it is suggested that the basic physical principals for the flow regime are incorporated in the proposed model.

Firstly with regards to the breakdown of the initial vortex sheet formed between the flow emerging from the blowing slot and the upper surface boundary-layer: the stability of this sheet is probably a function of blowing coefficient, slot height and the upper surface boundary-layer.

Secondly the size of the discrete vortices formed following the breakdown of the sheet is primarily a function of the lip geometry, while the shedding frequency is dependent upon the stability of the vortex sheet.

Thirdly the decay rate constant K, is a parameter which can be considered to represent entrainment. However it is not the main controlling parameter for determining the decay of the vortex structure. That is done by the vortex pairing process.

Finally there is circumstantial evidence to suggest that the TE separation point does not relate directly to lift as is the case with conventional potential flow theory. The analysis for predicting lift (see section 3.5) infers that lift due to blowing can be equated with the vortex strength and is independent of the vortex path. The separation point however is very much influenced by the proximity of the discrete vortices which are dynamic and continuously undergoing a seemingly random pairing process. This suggests that the separation point will be fluctuating. This would also be in accordance with the observations of Warsop and Marrero Santo(35) who were unable to determine the location of the separation point by hot-film shear stress measurements.[10]

---

7. The point X_{TE} lies at the intersection of the x-axis and the line perpendicular to the ellipse surface passing through the blowing slot location (not shown).
8. Augmentation rates dC_N/dC_μ from 30 to 40 are usual for this type of configuration.
9. Not included in this paper.
10. The frequency range of their instrumentation was well below the suggested vortex shedding frequencies.

5. *CONCLUDING REMARKS*

The model described in this paper needs to be considered in context with the earlier theoretical models which have been used for predicting the performance of CC-sections.

It is evident that the traditional use of an integral boundary-layer method combined with a finite difference technique around the TE does provide good overall performance results. However there is evidence to suggest that accurate prediction of the TE flow is still only partially successful.

As far as lift performance is concerned then errors in predicting the TE flow will have only marginal effect on the overall results. However when one is estimating the drag performance then the TE region is critical and an accurate theoretical method is required.

The proposed discrete vortex model shows distinct similarities with the observed flow field and it is suggested that discrete vortices may offer an alternative, or at the very least suggest improvements, to the finite difference methods which have been used to predict the *TE Coanda flow.*

REFERENCES

1	J.C. Eppel et.al	Static Investigation of the Circulation Control Wing/Upper Surface Blowing Concept Applied to the Quiet Short-Haul Research Aircraft. NASA TM 84232 (1982).
2	R.J. Englar G.G. Huson	Development of Advanced Circulation Control Wing High Lift Airfoils. AIAA Applied Aerodynamics Conference (1983). AIAA Paper 83-1847.
3	I.C. Cheeseman A.R. Seed	The Application of Circulation Control by Blowing to Helicopter Rotors. Journal of the Royal Aeronautical Society (1967). Vol.71, No.679.
4	E.O. Rogers	Recent Progress in Performance Prediction of High Advance Ratio Circulation Control Rotors. Presented at 6th European Rotorcraft and Powered Lift Aircraft Forum. Bristol, England (1980). Paper No. 29.
5	J.B. Wilkerson D.W. Link	A Model Rotor Performance Validation for CCR Technology Demonstrator. Presented at 31st Annual Forum of the American Helicopter Society (1975).
6	R.M. Williams	Application of Circulation Control Rotor Technology to a Stopped Rotor Aircraft Design. Presented at First European Rotorcraft and Powered Lift Aircraft Forum. Southampton, England (1975).
7	R.M. Williams R.T. Leitner	X-wing: A New Concept in Rotary Wing VTOL. Presented at the American Helicopter Society Symposium on Rotor Technology (1976).
8	I.C. Cheeseman	Circulation Control and its Application to Stopped Rotor Aircraft. The Aeronautical Journal (1968), Vol. 72, pp 635-646.
9	J. Dunham	Experiments Towards a Circulation Control Lifting Rotor Part I - Wind Tunnel Tests. The Aeronautical Journal (1970), Vol. 74, pp 91-103.
10	J. Dunham	A Theory of Circulation Control by Slot Blowing Applied to a Circular Cylinder. Journal of Fluid Mechanics (1968), Vol. 33, Part 3, pp 495-514.
11	E.S. Levinsky T.T. Yeh	Analytical and Experimental Investigation of Circulation Control by Means of a Turbulent Coanda Wall-Jet. NASA CR-2114 (1972).
12	R.J. Kind	A Calculation Method for Circulation Control by Tangential Blowing Around a Bluff Trailing Edge. Aeronautical Quarterly (1968), pp 205-223.
13	J.P. Ambrosiani	Analysis of a Circulation Controlled Elliptical Aerofoil. Aerospace Engineering (1971), TR-30.
14	E.H.Gibbs N. Ness	Analysis of Circulation Controlled Airfoils. Journal of Aircraft (1976), Vol 13, pp 158-160.

15	F.A. Dvorak	A Viscous Potential Flow Interaction Analysis for Circulation Controlled Airfoils. Analytical Methods (1978). Report No.7710.
16	F.A. Dvorak R.J. Kind	Analysis Method for Viscous Flow Over Circulation Controlled Airfoils. Journals of Aircraft (1979), Vol. 16. No. 1.
17	H.Schlichting	Boundary-Layer Theory 4th Ed. McGraw-Hill, New York (1960), pp.147-151.
18	H.Curle	A Two Parameter Method for Calculating the Two-Dimensional Incompressible Laminar Boundary-Layer. Journal of the Aeronautical Society (1967). Vol.71.
19	M.Gaster	The Structure and Behaviour of Laminar Separation Bubbles. Aeronautical Research Council (1967). ARC 28-226.
20	P.S.Granville	The Calculation of Viscous Drag of Bodies of Revolution. David Taylor Model Basin (1953), Rept.849.
21	D.E.Coles	Measurements in the Boundary-Layer on a Smooth Flat Plate in Supersonic Flow. Jet Propulsion Laboratory (1953), Rept.20-69.
22	J.F.Nash J.G.Hicks	An Integral Method Including the Effect of Upstream History on the Turbulent Shear Stress. Proceedings Computation of Turbulent Boundary-Layers. AFOSR-IFP Stanford Conference (1968), Vol.1.
23	F.A. Dvorak D.A.Choi	The Analysis of Circulation Controlled Airfoils in Transonic Flows. AIAA (1981), paper 81-1270.
24	A. Jameson	Numerical Computation of Transonic Flows with Shock Waves. International Union of Theoretical and Applied Mechanics. Springer-Verlag, New York (1975), pp 384-414.
25	G.W. Brune J.W. Manke	An Improved Version of the NASA Lockheed Multi-Element Airfoil Analysis Computer Program. NASA CR-154323 (1978), pp 69-87.
26	J.E. Green D.J. Weeks J.W.F. Brooman	Prediction of Turbulent Boundary-Layer and Wakes in Compressible Flow by a Lag-Entrainment Method. Royal Aircraft Establishment TR-52231 (1972).
27	R.V. Smith	A Theoretical and Experimental Study of Circulation Control with Reference to Fixed-Wing Application. Ph.D Thesis (1978), Southampton University, England.
28	K. Kawahara H. Takami.	Numerical Studies of Two-Dimensional Vortex Motion by a System of Point Vortices. Journal of Physical Soc. of Japan (1973), pp. 247-253.
29	J.F.Hackett M.R.Evans	Vortex Wakes behind High-Lift Wings. AIAA Journal of Aircraft (1971), Vol.8, No.5, pp.334-340.
30	M.M.E. Soliman	A Theoretical Study of Circulation Controlled Aerofoils and Experimental Applications to a Symmetrical Aerofoil. MSc. Thesis (1980), Southampton University, England.
31	M.M.E. Soliman R.V.Smith I.C.Cheeseman	Modelling Circulation Control by Blowing. AGARD Conference Proceedings (1984). Paper No.7, AGARD CP - 365.
32	N.J.Wood J.F.Henderson	Wind-Tunnel Tests on a Circulation Controlled Section. Presented at 6th European Rotorcraft and Powered Lift Aircraft Forum. Bristol, England (1980). Paper No.30.
33	N.J.Wood	The Aerodynamics of Circulation Controlled Aerofoils. Ph.D Thesis (1981), Bath University, England.
34	C.W.Hustad	The Drag of a Circulation Controlled Aerofoil. Ph.D. Thesis (1986), Bath University, England.
35	C.Warsop G.Marrero Santo	Measurement of the Surface Shear Stress around the Trailing Edge of a Circulation Controlled Aerofoil. Project Rpt. No.526 (1981), Bath University, England.